UC Irvine
UC Irvine Previously Published Works

Title
Spatio-temporal analysis of the cerebral spontaneous oscillation

Permalink
https://escholarship.org/uc/item/47x5b1k9

Journal
Proceedings of SPIE, 5330(19)

ISSN
0277-786X

Authors
Choi, Jee H
Wolf, Martin
Toronov, Vladislav Y
et al.

Publication Date
2004-05-28

DOI
10.1117/12.548202

Copyright Information
This work is made available under the terms of a Creative Commons Attribution License, availalbe at https://creativecommons.org/licenses/by/4.0/

Peer reviewed

eScholarship.org Powered by the California Digital Library
University of California

Spatio-temporal analysis of the cerebral spontaneous oscillation

Jee Hyun Choi [a], Martin Wolf [b], Vlad Toronov [c], Antonios Michalos [a], and Enrico Gratton [a]

[a] Laboratory for Fluorescence Dynamics, University of Illinois at Urbana-Champaign, 1110 W. Green Street, Urbana, IL 61801, USA;
[c] Clinic for Neonatology, University Hospital Zurich, Frauenklinikstr 10, 8091 Zurich, Switzerland;
[c] Beckman Institute for Advanced Science and Technology, University of Illinois at Urbana-Champaign, 405 N. Mathews Avenue, Urbana, IL 61801, USA;

ABSTRACT

Cerebral vasomotion was studied on the human brain in vivo by use of multi-optode frequency domain near-infrared spectroscopy (NIRS). Vasomotion is a spontaneous oscillation with a frequency of 0.1Hz in the arterial flow. We investigated (1) the fluctuations of cerebral hemodynamics on the dynamical characteristics of cerebral vasomotion and (2) the dynamical coupling between vasomotion in the skin and brain.

We found that (1) vasomotion is temporal coherent at least for about 3min; (2) vasomotion observed from NIRS is low-dimensional chaotic with its fractal dimension of about 4.5; (3) vasomotion is spatially coherent with coherence length of about 1-2cm but cerebral vasomotion is dynamically independent from vasomotion in the skin.

Keywords: Vasomotion, Near-Infrared Spectroscopy, Cerebral Hemodynamics

1. INTRODUCTION

The determination of the optical properties of the brain is important in many fields of medicine and neuroscience, both for monitoring of physiologically important processes and localizing any brain activities. In particular, the measurement of hemoglobin concentrations in the brain can provide important information about the cerebral oxygenation or related to neurovascular coupling. In near-infrared region, the light is highly scattering and low absorbing and the main chromospheres in biological tissue are oxy- and deoxyhemoglobin molecules. The spectral studies of the human brain using the near-infrared spectroscopy (NIRS) have been developed recently [1-3] and the baseline values of the oxy- and deoxyhemoglobin concentration of the adult human brain have been successfully measured using multi-optode frequency-domain NIRS separated from the scalp noninvasively [4].

The frequency-domain NIRS monitors the dynamical changes in the hemoglobin parameters continuously. Generally, the measured signals are fluctuating a lot with multiple sources and their spectral analysis show rich structure in the frequency domain. The frequency components in the spectral analysis are variable depending on the individual, but mainly we observe primary frequencies around 1, 0.3, 0.1, and 0.04 Hz corresponding to pulse, breathing, vasomotion, and the blood pressure wave, respectively. The rhythms, except 0.1Hz, are systemically driven or controlled by the central nervous system [5, 6], whereas the origin of vasomotion is still unknown but it exists in the entire body. Vasomotion is a rhythmic alternation of vasoconstriction and vasodilation of vessels, which is observed in the diameter measurement of the large and small arteries, and arterioles. It has been showed that 0.1Hz oscillation in NIRS is due to vasomotion by many researchers [7-9] .

In the NIRS signals, the amplitude of vasomotion is about 1-10 fold amplitude of the pulse and the frequency of it is variable but narrowly banded within the frequency band of 0.1±0.04Hz. In the diameter measurements, the patterns of vasomotion are variable depending on the types of arteries and measurement point [10] and the dynamics of vasomotion is determined to be highly nonlinear [11]. The spatial averaging of the NIRS signal is much larger than the spatial unit of the artery network, and therefore it is more reasonable to assume that the slow oscillation is the superposition of numerous vasomotion waves rather than an individual vasomotion at the level of single arteries. Therefore, the 0.1Hz oscillation observed in the NIRS signals is a collective vasomotion wave.

Complex Dynamics, Fluctuations, Chaos, and Fractals in Biomedical Photonics, edited by Valery V. Tuchin,
Proceedings of SPIE Vol. 5330 (SPIE, Bellingham, WA, 2004) · 1605-7422/04/$15 · doi: 10.1117/12.548202

Downloaded From: http://proceedings.spiedigitallibrary.org/ on 08/29/2016 Terms of Use: http://spiedigitallibrary.org/ss/termsofuse.aspx

Vasomotion in the brain is particularly interesting with its dynamic coupling with brain activation. Recently, Cimponerin and Kaplan [12] observed from the optical imaging of the cat visual cortex that vasomotion is stimulus-dependent. According to their observation, the spatially asynchronous vasomotion became spatially coherent at the start of stimulus as well as phase-locked to the stimulus. This is direct evidence that vasomotion is sensitive to neuronal activation and the phase-locking phenomena suggest that the relation between the neurovascular coupling and vasomotion is nonlinear. In addition, Diehl et al. [13] suggest the phase shift of cerebral vasomotion to the blood pressure wave as a measure of cerebral flow autoregulation, Biswal et al. [14, 15] and Lowe et al. [14, 15] even try to find a criterion for a functional connectivity map based on the correlation of spontaneous vasomotion. Most of all, the coupling behavior of cerebral vasomotion to the neuronal activation arises as an interesting subject with the increased interest in the area of the functional brain mapping. Usually, the cerebral vasomotion and neurovascular coupling are observed to interact with each other in a complicated manner so that the cerebral vasomotion is introduced as an intrinsic artifact in analyzing signals from neurons and it is challenging to filter.

In this manuscript, we focus on defining the dynamic characteristics of vasomotion in the cerebral hemodynamics assessed by frequency domain NIRS.

2. METHODS

2.1. Multi-optode frequency domain near-infrared spectroscopy

The propagation of light in tissue is well described by the diffusion equation for semiinfinite [16] or two-layer media [17]. Fantini et al. have obtained the analytic solution for the frequency domain parameters such as the average intensity I, modulation amplitude M, and phase shift ϕ., as functions of the distance ρ in a semiinfinite geometry boundary condition using the diffusion approximation [17]:

$$\frac{d\phi}{d\rho} = (\mu_a / D)^{1/2}\left[1 + (\omega / \mu_a v)^2\right]^{1/4} \sin\left[\tan^{-1}(\omega / \mu_a v)/2\right], \quad (1)$$

$$\frac{d\ln(\rho^2 M)}{d\rho} = -(\mu_a / D)^{1/2}\left[1 + (\omega / \mu_a v)^2\right]^{1/4} \cos\left[\tan^{-1}(\omega / \mu_a v)/2\right], \quad (2)$$

where D is the photon diffusion coefficient determined by $D = \left(2(\mu_s' + \mu_a)\right)^{-1}$, ω is the angular frequency of the modulation, v is the speed of light in the medium. From Eqs. (1) and (2), one can estimate μ_a and μ_s':

$$\mu_a(\rho) = \frac{\omega}{2v}\left(\frac{\partial_\rho \phi}{\partial_\rho \ln\left[\rho^2 M(\rho)\right]} - \frac{\partial_\rho \ln\left[\rho^2 M(\rho)\right]}{\partial_\rho \phi}\right), \quad (3)$$

$$\mu_s'(\rho) = \frac{\left(\left(\partial_\rho \ln\left[\rho^2 M(\rho)\right]\right)^2 - (\partial_\rho \phi)^2\right)}{3\mu_a} - \mu_a, \quad (4)$$

where $\ln\left[\rho^2 M(\rho)\right]$ and $\partial_\rho \phi$ are the slopes of modulation and phase shift with respect to ρ. Using Eqs. (3) and (4), μ_a and μ_s' can be determined directly from the values of ϕ and M measured at ρ in the frequency domain. One benefit of these expressions is their independence from the instrumental parameters such as the laser light power, detector sensitivity, and other instrumental factors. However, since the above equations were obtained under the assumption that the amplitude and initial phase are the same for each light source, an instrumental calibration must be performed to correct for any inequalities in the amplitude and phase by calibration with a tissue phantom with known optical properties.

According to Beer-Lambert law, the absorption coefficient can be written as a linear sum of the extinction coefficients multiplied by the concentration of absorber and in the near infrared region, oxyhemoglobin (c_{oxy}) and deoxyhemoglobin (c_{deoyx}) are main absorber. Therefore the absorption coefficient is represented by

Downloaded From: http://proceedings.spiedigitallibrary.org/ on 08/29/2016 Terms of Use: http://spiedigitallibrary.org/ss/termsofuse.aspx

$$\mu_a^{\lambda} = \sum \varepsilon_i^{\lambda} c_i \cong \varepsilon_{oxy}^{\lambda} c_{oxy} + \varepsilon_{deoxy}^{\lambda} c_{deoxy} \,. \quad (5)$$

where ε_i is the extinction coefficient of the ith chromophor. Since the μ_a and ε are dependent on wavelength of light, we can solve eq. (5) by use of two wavelengths of light.

2.2. Experimental Methods

The instrumental configuration used in determining the hemoglobin parameters is schematically shown in Figure 1. We used a multi-channel frequency domain near infrared spectrometer (Imagent, ISS, Champaign, IL). In brief, the instrument employs laser diodes (LD) modulated at the frequency, 110MHz and photomultiplier tubes (PMT) whose gain is modulated at a close frequency of 110.005MHz to heterodyne the high frequency down to the frequency of 5 kHz. In this study, 32 LDs (16 at 758nm and 16 at 830nm) and our PMTs were used. The LDs were multiplexed so that two LDs with the same wavelength and at the same location were on at a time. The light from LDs was guided by the optical fibers with a diameter of 400 μm to the tissue surface and the photons re-emitted from the tissue were collected simultaneously by the fiber bundles with a diameter of 5.6 mm placed several centimeters apart from the source fibers. The collected light was carried to the PMTs and then the signals from the PMTs were digitally processed to yield I, M, and ϕ.

We investigated the time series of oxyhemoglobin concentration (c_{ox}) as the vasomotion parameter of interest. Data were obtained from an adult forehead with multidistance frequency domain NIRS probe (source-detector distance 1-8cm) at data acquisition frequency of 2.5Hz.

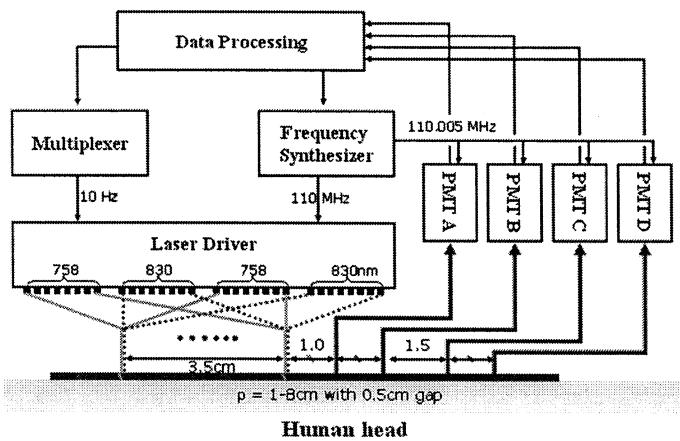

Figure 1 Block diagram of frequency-domain near-infrared spectroscopy (Oxy-Imager ISS, Champaign, IL USA) and geometric arrangement of the long-ranged multi-distance probe containing the source and detector fibers on the forehead.

2.3. Data analysis

2.3.1. Pattern recognition

A repeatability of a similar pattern in a time series can be characterized by pattern recognition. We use the least squares method to fit a part of interest to the entire time series. To illustrate the linear squares fitting process, suppose one has a test data set $\{y_i\}$ with a size of N that can be fitted to a reference data set $\{x_i\}$ with the same size. We may model the reference data by a first degree polynomial such as $y = px+q$, whereas p and q are fitting coefficients.

We solve the equation for the unknown coefficients p and q with a least squares fitting process by minimizing the normalized summed squares of the residuals $\chi^2(p,q)$, i.e.

Downloaded From: http://proceedings.spiedigitallibrary.org/ on 08/29/2016 Terms of Use: http://spiedigitallibrary.org/ss/termsofuse.aspx

$$\chi^2(p,q) = \frac{\sum_{i=1}^{N}(y_i - (px_i + q))^2}{N\sigma_y{}^2}, \quad (6)$$

where N is the length of the data and σ_y is the sample variance of the data yi. The minimized summed squared residual $\chi^2(p,q)$ is solved by $d\chi^2(p,q)/dp = 0$ and $d\chi^2(p,q)/dq = 0$. Using this method, one can recognize a particular pattern in a time series by scanning the whole data with the pattern. If the data is the same as the pattern, χ^2 will be zero. On the contrary, if one fails to interpolate the data with the pattern, the minimized χ^2 will be a constant function with the mean value of data, therefore, χ^2 will be zero by definition.

2.3.2. Cross-correlation study

One effective way to describe the joint properties of two time series is the cross correlation function. It describes the general dependence of one signal to the other. For two time sequences, $x(t)$ at time t and $y(t)$ at time $t+\tau$ for an observation period T, a cross correlation function is defined by

$$CCF(\tau) \equiv \lim_{T\to\infty} \frac{1}{2T} \int_{-T}^{T} x(t)y(t+\tau)dt. \quad (7)$$

The cross correlation function $CCF(\tau)$ indicates the existence of correlation between $x(t)$ and $y(t)$ for a specific time displacement, τ. Therefore, the maximum of $CCF(\tau)$ will yield the time delay of $y(t)$ with respect to $x(t)$.

A cross correlation function within the same signal is called the autocorrelation function. The autocorrelation function for random data provides a general temporal structure of a time series by evaluating the dependence of the value of the time series at one time on the value at another time. Intuitively, it is a measure of how similar a series is with a shifted version of itself. This autocorrelation function is an even function by definition and has a global maximum at the origin, i.e. $\tau = 0$. The major application of an autocorrelation function is to monitor the influence of a value at any time to values at a future time. For example, a noisy signal without any deterministic nature has a quickly decaying $ACF(\tau)$ as τ increases. Whereas, if the signal is deterministic, $ACF(\tau)$ will exist over all τ and have local peaks at every period of oscillation modes. Hence, $ACF(\tau)$ is very useful for detecting a characteristic frequency buried in an extraneous noise. If $CCF(\tau)$ of two independent time series is similar to $ACF(\tau)$ of one, the signals are coherent to each other.

2.3.3. Fractal dimension

The fractal dimension is a magnification factor of self-similar objects in a fractal geometry that is defined by D_f = log(number of self-similar unit)/log(magnification factor). Basically, it is a measure of how complicated a self-similar pattern is. This concept may also be applied for determining the dynamic characteristic of a time series. In case of a time series, D_f can be the degree of freedom of the dynamical system that the series belongs to and it is a measure of strange attractors if the system is deterministic chaos [18]. If the time series is completely random, D_f will be infinite whereas if the time series is a deterministic signals, D_f will be a finite number.

A popular method to calculate a fractal dimension in time series analysis is the correlation dimension D_c:

$$D_c \equiv -\lim_{r\to 0} \frac{\log C(r)}{\log(f)}, \quad (8)$$

where C(r) is the number of points of the set located within a smaller distance of the values than a given distance r (correlation integral). The correlation integral C(r) is defined as

$$C(r) \equiv \lim_{N\to\infty} \frac{1}{N^2} \sum_{\substack{i,j=1 \\ i\neq j}}^{\infty} H(r - |x_i - x_j|), \quad (9)$$

Downloaded From: http://proceedings.spiedigitallibrary.org/ on 08/29/2016 Terms of Use: http://spiedigitallibrary.org/ss/termsofuse.aspx

where H is the Heaviside step function (H(s) = 1 for s>0 and H(s) = 0 for s<0). For example, a distance r can be arbitrarily chosen and $C(r)$ can be evaluated by counting the number of points of the neighborhood in the experimental data that falls into the distance r. And the slope in a plot of log $C(r)$ versus log (r) as r goes to zero will be equal to D_c.

However, in practice, the experimental data are not continuous but discrete and D_c will yield different values for different time scale. Therefore, a reliable way to evaluate D_c is to calculate D_c for different time scales and find a value that remains constant regardless of the change of the time scale. The time scale can be easily modified by multiplying an integer m in the time index $x_i \rightarrow x_{mi}$ and usually, m is called an embedding dimension. Then the correlation dimension for this embedding dimension m, $C(r,m)$ is calculated by

$$C(r,m) \equiv \lim_{N\to\infty} \frac{1}{N^2} \sum_{\substack{i,j=1 \\ i\neq j}}^{\infty} H(r - |x_{mi} - x_{mj}|). \quad (10)$$

If the time series is noisy, $C(r,m)$ will increase with increasing m without ever reaching a plateau. But if the time series is deterministic, $C(r,m)$ will reach a plateau for a time scale larger than a certain value of m because of its characteristic of self-similarity. And the plateau value of $C(r,m)$ is the fractal dimension of the time series.

3. RESULTS

3.1. Dynamical characteristics of cerebral vasomotion

3.1.1. Temporal structure

We first estimated the temporal coherence based on the pattern recognition method. The temporal coherence measures the correlation of two distant events in a time series. We used the nonfiltered data after detrending with a 3rd order polynomial function (Figure 2(a)). Figure 2(b) shows the result from the pattern recognition method. For the pattern recognition analysis, we randomly picked a time window with a size of 10sec and scanned the entire time series and evaluated the summed square of the residuals χ^2(t). The local minima indicate the appearance of a similar pattern. A detailed analysis of χ^2(t) shows that local minima tend to be separated by a period of 15 sec and that this behavior persists with time. The local minimum does not appear at every vasomotion period but appears repetitively.

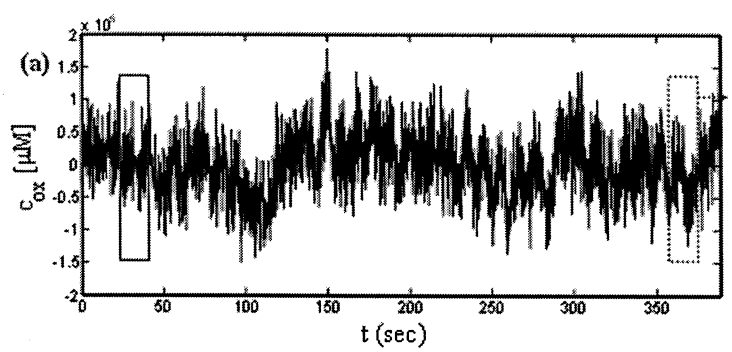

Downloaded From: http://proceedings.spiedigitallibrary.org/ on 08/29/2016 Terms of Use: http://spiedigitallibrary.org/ss/termsofuse.aspx

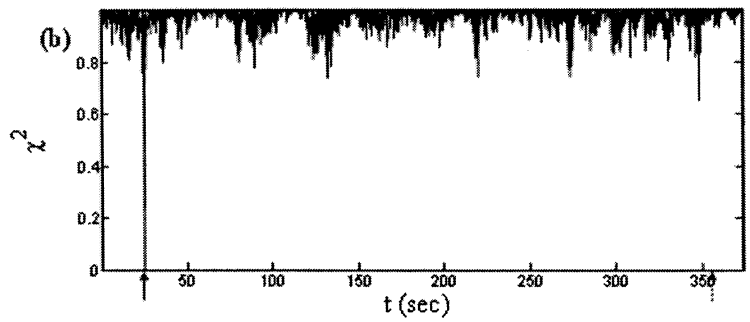

Figure 2 (a) Oxyhemoglobin fluctuation recorded from the forehead of an adult. The solid line box contains the reference signal for the pattern recognition test and the dotted box move the entire time to produce $\chi 2$ (b). $\chi 2$ of the least square method plotted with respect to the time. The solid/dotted arrow is the temporal location of the reference/test signal, respectively.

We next use the autocorrelation analysis to determine the long range dependence of the vasomotion wave. Figure 3 (a) shows ACF of the same time series in Fig. 2(a). Figure 3 (b) shows the same function in a smaller time window. The modulations of ACF with an approximate period of 10sec and other oscillations at longer periods are also observed. The main feature of Fig. 3 is that the ACF of the oxyhemoglobin signal decreases to zero slowly in an oscillatory behavior conserving the long range dependence lasting for a significant amount of time (> 3min).

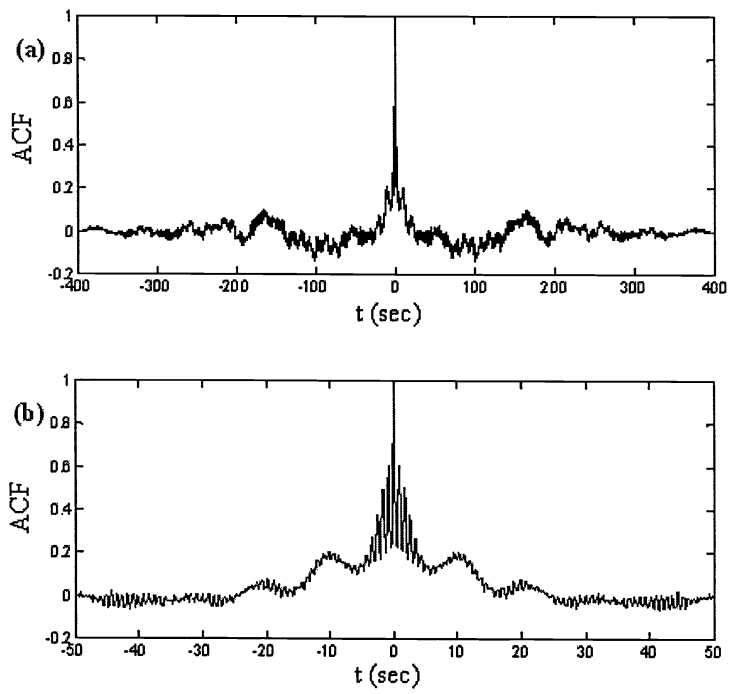

Figure 3 (a) The autocorrelation of the oxyhemoglobin after a polynomial detrending plotted for the whole period of time. (b) The same function plotted in smaller time window.

Downloaded From: http://proceedings.spiedigitallibrary.org/ on 08/29/2016 Terms of Use: http://spiedigitallibrary.org/ss/termsofuse.aspx

3.1.2. Fractal dimension

The fractal dimension of the vasomotion was calculated using the Grassberger-Procaccia method [18]. We first chose a time delay of 2.5sec that is approximately ¼ of the vasomotion period. The correlation integral $C(\varepsilon,m)$ was obtained by Eq. (10) by calculating the probability that the pair of neighboring points has a distance smaller than ε for an embedding dimension m. The correlation dimension was obtained from the slope by a linear regression in the linear region with distinct slopes of log $C(\varepsilon,m)$. The correlation dimension D_c was plotted with respect to the embedding dimension m in Fig. 4. In order to test the dependency of the fractal dimension on the time delay τ, we plotted D_c for different values of τ in Fig. 4. Each plot of D_c versus m reaches a plateau and its value is similar. The value at the plateau is taken as the estimate of the fractal dimension D_f and a fractal dimension of about 4.5 is suggested from this plots.

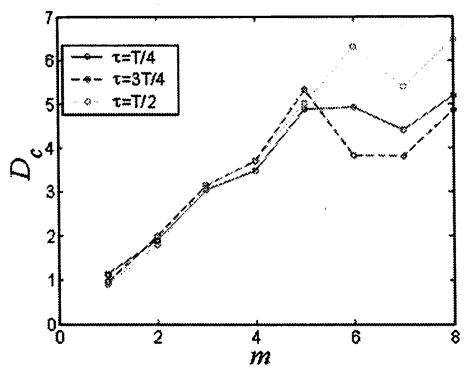

Figure 4 The correlation dimension, D_c as a function of embedding dimension, m for different time delay τ. The solid, dashed, and dotted lines are $D_c(m)$ for τ = T/4, 3T/4, and T/2, respectively, where T is the period of vasomotion (~10sec).

3.2. Spatial correlation

We analyzed a set of data spatially distributed in the vertical section into the brain to extract information on the dynamical correlation between vasomotion at the skin and the brain surface. The data was obtained from the forehead of an adult with the multidistance probe ranging from 1-8cm of its source-detector distance. Visualizing the correlation between vasomotion is very difficult, when we do not filter the data, because the fluctuation amplitudes of the other physiological signal such as pulse and blood pressure wave are comparable to the vasomotion. Therefore, we filtered the vasomotion with 5th order of Butterworth bandpass filter with passband from 0.06Hz to 0.20Hz and stopband from 0.02Hz to 0.28Hz. Since the phase difference between two parameters is one of our interests, we used zero-phase filtering by processing the input data in both the forward and reverse direction [19].

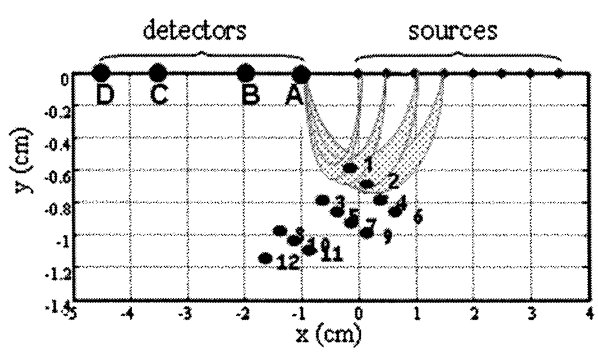

Figure 5 The region of sensitivity for long-ranged multidistance NIRS signal. The horizontal axis is the surface of the forehead and the vertical axis is the depth from the tissue surface. The NIRS signal at each position is obtained from the slopes of

Downloaded From: http://proceedings.spiedigitallibrary.org/ on 08/29/2016 Terms of Use: http://spiedigitallibrary.org/ss/termsofuse.aspx

the modulation and the phase shift with respect to the source-detector distance for 4 sources.

From the given probe, the approximate region of maximal signal sensitivity is shown in Fig. 5 and the penetration depth z is determined by $z = r^{1/2}\left(3\mu_a\mu_s'\right)^{-1/4}/2$ [20]. We denote the filtered oxyhemoglobin contents at the nth position as $c_n(t)$. n=1 indicates the closest point to the skin and as n increases, the measurement point goes deeper. In order to investigate the spatial correlation between vasomotion signals at different depths with the aim of describing the dynamical feature of the propagation of vasomotion waves, we use a cross-correlation technique. The cross-correlation $\chi_{n,m}$ between two simultaneously registered time series of $c_n(t)$ and $c_m(t)$ is determined by Eq. (7) For all the possible pairs, we draw the cross-correlation map of a test signal $c_n(t)$ with the reference signal . By simple visual inspection of the cross-correlation plots, we joined all the regions that have similar cross-correlation to the autocorrelation at a given location, which indicate that the patterns of slow oscillations are similar at that location. We obtained the map shown in figure 6. A clear pattern of local spatial coherence appears localized into topologically distinct and non-intersecting regions.

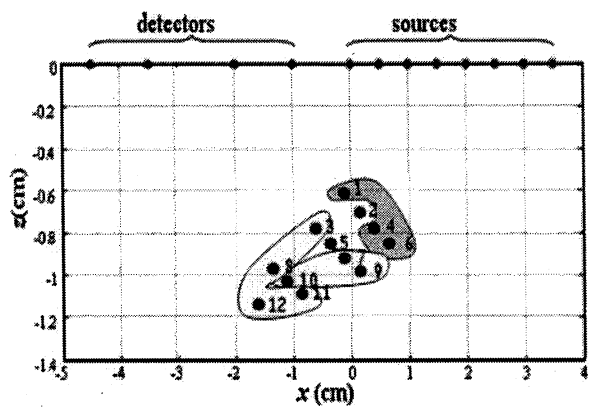

Figure 6 Topological map of the regions that have similar cross correlation to the autocorrelation at a given location.

4. DISCUSSION AND CONCLUSION

Both the pattern recognition and autocorrelation analysis show that similar patterns are repeating with the frequency of vasomotion and the correlation dissipates slowly with time. This analysis clearly shows that the long range dependence of the vasomotion is not limited to a few periods of vasomotion but exists for dozens of periods. In other words, the vasomotion wave is a temporally coherent wave even though there is no explicit driving force of the fluctuation.

The finite fractal dimension suggests that the dynamics of vasomotion belong to a low-dimensional dynamical system. If the vasomotion is stochastic, D_c will increase continuously without reaching a plateau with m. It is interesting that the fractal dimension we obtained is similar to those obtained from diameter measurements. Rosen et al. [21] calculated the fractal dimension of the diameter and red blood cell velocity in a single vessel. Fractal dimensions of 3-4 were obtained for diameter oscillations and that of 6-7 for velocity oscillations in the same vessel. Slaaf et al. [22] also obtained the fractal dimension of about 4 in the diameter measurement. The signal from NIRS is a volumetric parameter measuring the amount of fresh blood in the arteriole network in a tissue. Therefore, it is reasonable that our result is similar to those for the diameter measurement rather than the flow measurement. However, the vasomotion results from NIRS are statistically averaged over a large scale of arteriole networks, merging the individual vasomotion at a number of arterioles. If any contribution from an arbitrary dynamical factor is added or removed during the signal integration, the

Downloaded From: http://proceedings.spiedigitallibrary.org/ on 08/29/2016 Terms of Use: http://spiedigitallibrary.org/ss/termsofuse.aspx

fractal dimension will increase or decrease. We obtained a similar value of the fractal dimension, which implies the dynamical property is conserved throughout the arteriole network.

The cross correlation analysis on cerebral vasomotion measured in different locations at the forehead and in the motor cortex has shown that the cerebral vasomotion has a local spatial coherence extending to regions of 1-2cm in size.

REFERENCES

1. Villringer, A. and U. Dirnagl, *Coupling of brain activity and cerebral blood flow: basis of functional neuroimaging.* Cerebrovasc Brain Metab Rev, 1995. 7(3): p. 240-76.
2. Bevilacqua, F., et al., *In vivo local determination of tissue optical properties: applications to human brain.* Applied Optics, 1999. 38(22): p. 4939-4950.
3. Toronov, V., et al., *Near-infrared study of fluctuations in cerebral hemodynamics during rest and motor stimulation: temporal analysis and spatial mapping.* Med Phys, 2000. 27(4): p. 801-15.
4. Choi, J.H., et al., *Noninvasive determination of the optical properties of the adult human brain: frequency domain near-infrared spectroscopy approach.* Journal of Biomedical Optics, 2004. in press.
5. Malpas, S.C., et al., *The sympathetic nervous system's role in regulating blood pressure variability.* IEEE Eng Med Biol Mag, 2001. 20(2): p. 17-24.
6. Seydnejad, S.R. and R.I. Kitney, *Modeling of Mayer waves generation mechanisms.* IEEE Eng Med Biol Mag, 2001. 20(2): p. 92-100.
7. Mayhew, J.E.W., et al., *Cerebral Vasomotion: A 0.1-Hz Oscillation in Reflected Light Imaging of Neural Activity.* NeuroImage, 1996. 4(3): p. 183-193.
8. Obrig, H., et al., *Spontaneous Low Frequency Oscillations of Cerebral Hemodynamics and Metabolism in Human Adults.* NeuroImage, 2000. 12(6): p. 623-639.
9. Hudetz, A.G., et al., *Spontaneous fluctuations in cerebral oxygen supply. An introduction.* Adv Exp Med Biol, 1998. 454: p. 551-9.
10. Stergiopulos, N., et al., *Arterial vasomotion: effect of flow and evidence of nonlinear dynamics.* Am J Physiol Heart Circ Physiol, 1998. 274(6): p. H1858-1864.
11. Griffith, T.M. and D.H. Edwards, *Complexity of chaotic vasomotion is insensitive to flow and pressure but can be regulated by external control.* Am J Physiol Heart Circ Physiol, 1995. 269(2): p. H656-668.
12. Cimponeriu, A. and E. Kaplan. *Evoked and spontaneous vasomotion revealed by optical imaging of intrinsic signals on the cat primary visual cortex.* in *ARVO*. 2001.
13. Diehl, R.R. and P. Berlit, *[Quantitative tilt table study with TCD monitoring. A reliable method for the diagnosis of neurocardiogenic syncope (vasovagal syncope)].* Nervenarzt, 1995. 66(2): p. 116-23.
14. Biswal, B.B., J. Van Kylen, and J.S. Hyde, *Simultaneous assessment of flow and BOLD signals in resting-state functional connectivity maps.* NMR Biomed, 1997. 10(4-5): p. 165-70.
15. Lowe, M.J., B.J. Mock, and J.A. Sorenson, *Functional connectivity in single and multislice echoplanar imaging using resting-state fluctuations.* Neuroimage, 1998. 7(2): p. 119-32.
16. Fantini, S., et al., *Frequency-Domain Multichannel Optical-Detector for Noninvasive Tissue Spectroscopy and Oximetry.* Optical Engineering, 1995. 34(1): p. 32-42.
17. Kienle, A., et al., *Noninvasive determination of the optical properties of two-layered turbid media.* Applied Optics, 1998. 37(4): p. 779-791.
18. Grassberger, P. and I. Procaccia, *Measuring the strangeness of strange attractors.* Physica D: Nonlinear Phenomena, 1983. 9(1-2): p. 189-208.
19. Oppenheim, A.V. and R.W. Schafer, *Discrete-Time Signal Processing*. 1989: Prentice-Hall.
20. Patterson, M.S., B. Chance, and B.C. Wilson, *Time Resolved Reflectance and Transmittance for the Noninvasive Measurement of Tissue Optical-Properties.* Applied Optics, 1989. 28(12): p. 2331-2336.
21. Rosen, B., C. Tahedel, and B. M. *Correlation dimension analysis of vascular diameter and red blood cell velocity in microvessels.* in *World Congr Microcirc*. 1991. Louisville, KY.
22. Slaaf, D.W., et al., *Nonlinear Dynamics of Vasomotion.* Prof Appl Microcirc., 1993. 20: p. 67-80.

Downloaded From: http://proceedings.spiedigitallibrary.org/ on 08/29/2016 Terms of Use: http://spiedigitallibrary.org/ss/termsofuse.aspx